Classifying Landslides Using LiDAR-based DEMs

Virginia Latane

Supervised by Dr. Marco Millones

23 July 2020

University of Mary Washington

GIS Capstone Project

Introduction

On the night of 19-20 August 1969, Hurricane Camille dumped 27" of rain over Nelson County over 8 hours. The high rainfall over a relatively short time period triggered fast-moving debris flows that began on the hillslopes and converged with the flash floods already happening below. The event claimed ~124 lives in Nelson County (Witt and Whitehead 2019). The property damage was extensive across affected areas in Virginia. The hillsides of Nelson County still bear scars of the catastrophic weather event today.

The debris flows and debris slides caused by Hurricane Camille are landslides. A landslide is a downslope movement of soil, rock, or earth mass. Landslides result from different triggers, can be rapid or slow moving, and produce a wide variety of geomorphic landforms in the aftermath (Highland and Bobrowsky 2008). One commonality of many landslides is their destructive nature. According to the U.S. Geological Survey (USGS), across the United States, landslides kill an average of 25-50 people and cause $2-4 billion worth of property damage annually (Landslides 101, n.d.).

This paper will focus on landslides triggered by the heavy rainfall of Hurricane Camille in Nelson County, Virginia. Many of these landslides produced a diagnostic landform that begins with a relatively narrow, curved head scarp, transitions into a narrow, long debris track, and ends with a downslope deposit of freshly removed and mobilized material. Figure 1. shows the generalized pattern of these features. See Figure 2. for real world examples.

The Virginia Department of Mines, Minerals, and Energy (VA DMME) is compiling a Virginia Landslide Database, to track and study landslides that occur and have occurred across the Commonwealth. The database contains thousands of slides in the region of Nelson and Albemarle Counties, collected under a FEMA grant awarded for the purpose of studying Hurricane Camille-caused landslides in this area.

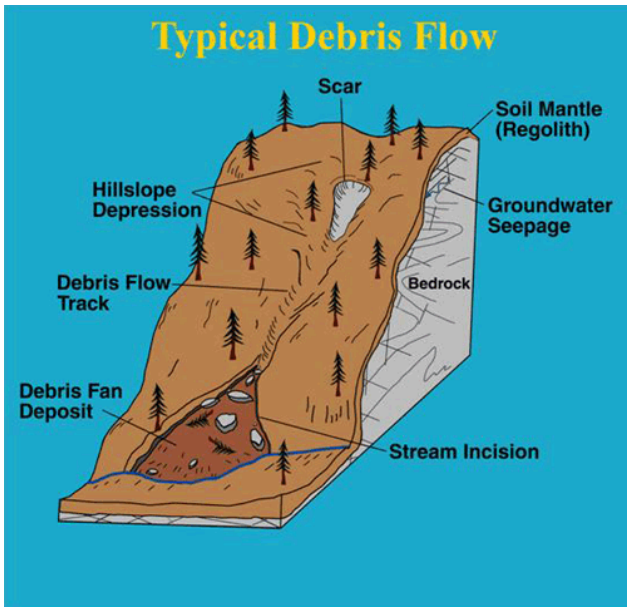

Figure 1. Parts of a typical debris flow. Image from Rick Wooten, North Carolina Geological Survey *in* Witt and Whitehead 2019.

Landslides and landslide deposits are partially studied for the end goal of landslide prediction. Modeling begins with a landslide inventory. Inventories are compilations of ancient, historical, and up-

to-the-moment landslide information that is field verified. In this case, VA DMME compiled many landslide features from pre-existing sources such as USGS papers, but locations have been updated, refined, and added based on 2016 LiDAR.

As with many datasets, the foundation of a landslide inventory is manual work performed by a technician or analyst. These workers typically rely on visual identification and interpretation. Results can vary greatly depending on experience, training, and number of workers. In general, adding to an inventory using tradition methods is time consuming and costly.

This project seeks to find a starting point for a landslide inventory that is not based on manual identification, but instead on the semi-automated process of classification.

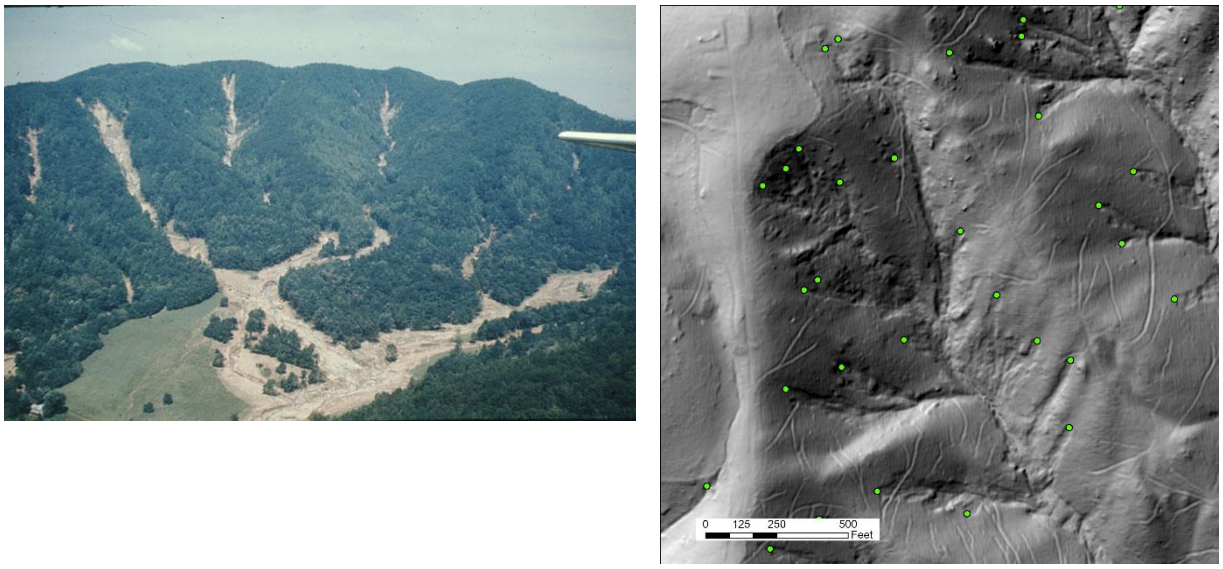

Figure 2. *Left,* Tan colored debris flows triggered by Hurricane Camille in Fortune's Cove (photograph from VA DMME). *Right,* Landslide scars visible in a different part of Fortune's Cove. Landslide initiation points indicated by green dots.

Data

This study relies primarily on Digital Elevation Models (hereafter referred to as “DEMs”) produced from LiDAR. These 1-m resolution DEMs are available pre-processed and distributed by the USGS through The National Map (TMN). The LiDAR data was flown in 2015-2016 and was produced as part of the USGS 3D Elevation Program (3DEP) in partnership with the Virginia Geographic Information Network (VGIN). These DEMs form the basis for all elevation-based products used in this study. I acquired six DEM tiles to fully cover my study area.

Secondary datasets came from the VA DMME. At the outset of the project, I acquired a feature class showing landslide feature initiation points across this study area. This point feature class,

known as “process points” contains initiation points compiled from different reports, as well as points identified by technicians using LiDAR-based slope-shade and hill-shade maps, aerial orthophotography, and other sources. Not all points are ground-truthed or field verified. Many points compiled from other sources have been moved to adjust for differences in resolution and scale between the source material and the LiDAR-based DEMs.

Midway through the project, I acquired a polygon feature class from VA DMME known as “slope movement outlines”. These polygons represent the outlines of the entirety of landslide features, from initiation point to downslope deposit. This dataset, like process points, is also compiled from multiple sources. These outlines were created to reflect the original extent of Hurricane Camille landslide features at the time of the event. This dataset is still in draft form. In some cases, these outlines were originally drawn using a coarser resolution DEM. In other cases, the outlines simply need further refinement. Collection of landslides in this area is part of an ongoing project.

I also used two feature datasets for river and road layers. I downloaded vector stream and river data from the National Hydrography Dataset (NHD). This polyline dataset was developed at 1:100,000 scale for nationwide use; the Virginia portion was last updated in April 2019. In this area, the only applicable features from this dataset are known as “flowlines”, which are basically unordered streams. This data is delivered to the public via VGIN. I also downloaded a Virginia Road Centerlines shapefile from VGIN’s repository. This dataset contains regularly updated polyline features that represent U.S., state, and local roads.

Study Area

This study is contained within 90 mi^2 across two USGS 7.5’ quadrangles, Horseshoe Mountain and Sherando, in Nelson County, Virginia (Figure 3.) This area contains hillsides that collapsed during Hurricane Camille, producing thousands of debris flow head scarps across the two quadrangles. The full extent of the damage caused by Hurricane Camille in Nelson and Albemarle Counties covers a much broader areal extent; the features within this study area represent only a subset of the Camille caused landslide features tracked within the Virginia Landslide Database.

Nelson County in general was selected because of its visible landslide features, and because 2016 1-m resolution LiDAR is freely and publicly available for the entirety of the county. These specific quadrangles were chosen because they differ from each other in terms of general topography and human modification. Though topographical differences between the two quadrangles imply a difference in geology, geological differences are not examined in this study.

Together, these quadrangles represent both slide-heavy and slide-scarce areas affected by Hurricane Camille.

Topographically, this portion of Sherando Quadrangle is flatter than Horseshoe Mountain. Much of the southern part is composed of a broad, flat swaths of land where the possibility of landslides is unlikely. Many of the flat areas are agricultural fields. It also includes the popular leisure destination Wintergreen Resort, as well as the community of Nellysford. Overall, a higher proportion of this quadrangle has been modified by humans than in Horseshoe Mountain. Proportional to its area, Sherando contains fewer landslide features than Horseshoe Mountain.

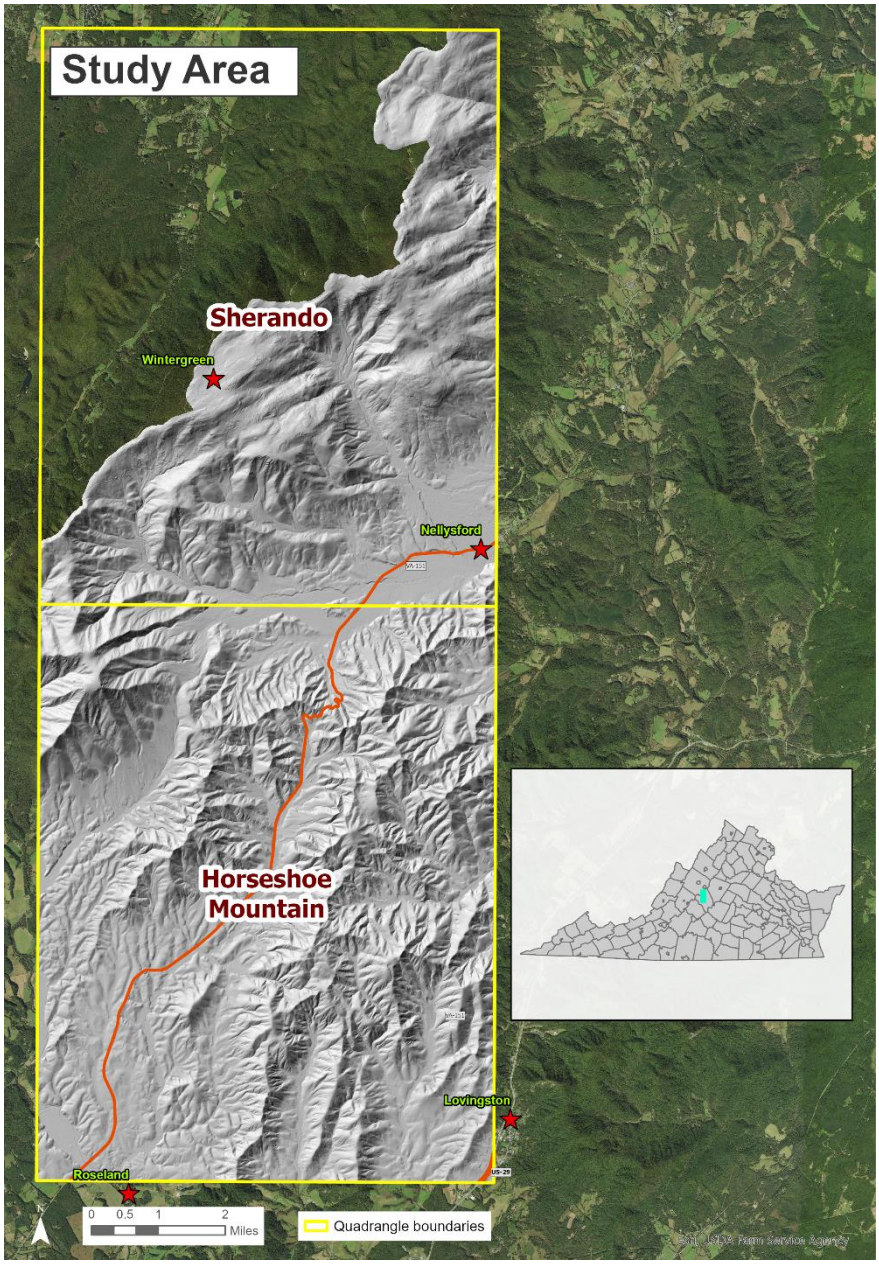

Figure 3. Study Area in hill-shade overlaid onto NAIP imagery.

Like Sherando, Horseshoe Mountain contains large flat areas that have been partially modified for agricultural use, particularly in the southwest quadrant. However, it also contains many rugged, steeply sloped hillsides that are not seen in Sherando. The town of Lovingston and community of Roseland lay partially within its borders, but the steep terrain in the majority of Horseshoe Mountain shows fewer signs of dense human occupation and modification. Overall, Horseshoe Mountain has a higher landslide density than Sherando.

Methodology

Landslide features are visible in LiDAR-based DEM "derivatives" (hereafter referred to as "DEM-derivatives"), such as hill-shade and slope-shade maps. These features are also visible on orthophotography and uncorrected aerial photography. A robust manual interpretation uses several vintages of photography in conjunction with elevation data to identify the full extent of a landslide feature. The aerial photography is particularly important for revealing the extent of landslide deposits that have since been eroded by fluvial features or covered up by human modifications to the landscape, such as agricultural fields. That aerial imagery used by VA DMME was not used in this effort.

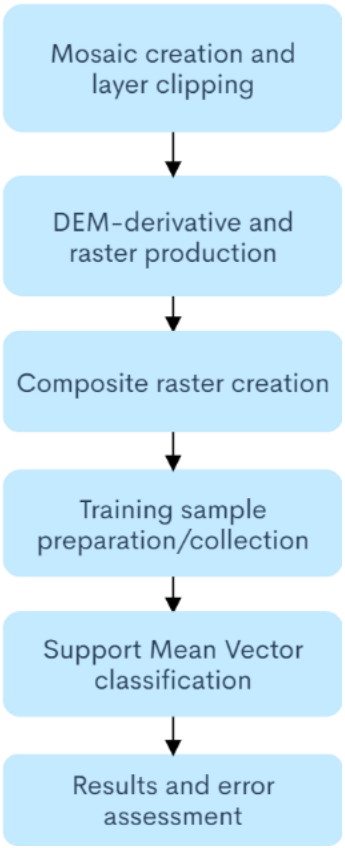

Figure 4. A generalized workflow for this study.

This study followed a pixel-based classification workflow. Pixel-based classification is commonly used in the creation of land cover classification maps using multispectral satellite imagery. In this study, I have used DEM-derivatives in place of that imagery, a tactic used by previous workers to identify landslides, albeit with different modelling methods (Pawłuszek et al. 2019, West Virginia Statewide Hazard Assessment - Landslide Risk Assessment 2019). An Object-Based Image Analysis (OBIA) was considered and tested for this study, but was abandoned due to time constraints. All methods detailed below were performed in ArcGIS Pro. Figure 4. shows a general progression of the steps laid out in detail below. A more typical classification workflow would include repeating these steps as needed until the desired product is reached.

Data Preparation

The 3DEP preprocessed DEMs arrive as discrete tiles. For the sake of consistency and efficiency I created a mosaic from the six tiles. The mosaiced tiles create a continuous grid of elevation data.

National Hydrologic Dataset flowlines are packaged at a National Scale. Virginia road centerline data is available at the state scale. These layers, as well as the DEMs and slope movement outlines, were clipped to the study area.

DEM-derivative, River and Road Raster Production

I chose seven different raster images to include in this classification. Broadly speaking, I chose these layers based on the results of previous studies (Pawłuszek et al. 2019, Statewide Hazard Assessment - Landslide Risk Assessment 2019). These layers were all produced in ArcGIS Pro. Because of limitations to both access and time, I opted to produce only derivatives that would not require using third-party toolboxes or non-ESRI GIS software. Some DEM-derivatives, such as slope, surface roughness, and curvature were chosen based on the clear visibility of landslide features within them.

1. Slope angle is one important factor that determines a hillside's propensity to collapse into a landslide. Slope-shade maps are a DEM-derivative used in visual interpretation of landslides. For this raster slope map, a 3 x 3 moving window was used to calculate the slope value for each pixel using the elevation values of it and its eight neighbors, and the set distance between adjacent pixels.

2. Surface roughness describes the variability of a surface across a given scale, which is a useful variable in geomorpohological analyses (Grohmann, Smith and Riccomini 2011). Here, it was calculated from the slope. I used the Focal Statistics tool to calculate the standard deviation of slope values within a range defined by a 3 x 3 moving window across the entirety of the map. Each pixel's value was equal to the standard deviation of the distribution of slope values in the surrounding eight pixels. The result was a map that displays the variability of slope as a continuous image.

3. Curvature is a measure of the concavity or convexity of a sloped surface. Curvature can be useful for picking out the distinctive cone shape of head a landslide's head scarp (Pawłuszek et al. 2019). In this study, landslide features beyond the scarp were clearly visible in the curvature map. Curvature maps generated in ArcGIS Pro can display curvature parallel to the direction of slope (planiform), perpendicular to the direction of slope (profile), or a combination of the two. I opted for the combination in this study.

4. Aspect can be considered equal to slope direction. It is calculated using a 3 x 3 window to identify the maximum rate of change within the eight surrounding pixels. A previous study determined that aspect was not useful in the examination of all Hurricane Camille landslides in Virginia (Witt and Whitehead 2019). However, given that this is a localized

subset of landslides, and that aspect has been used in previous landslide studies, it was still considered here.

5. Hill-shade maps display elevation data hypothetically lit from a particular sun azimuth (0-360) and a particular altitude (0-90). This type of map was included because it is a useful tool in visual interpretation.

6. I generated a river network for the study area using the flow direction and flow accumulation tools in ArcGIS Pro on the mosaiced DEMs. This multipart process consisted of calculating the direction water would flow over the surface, then calculating where it would collect based on the values of surrounding cells. The final product is reclassified to the level of detail slightly beyond that of the NHD lines.

7. Road density is one way to examine a relationship between landslides and road features. A road density raster was included here because previous studies have found a correlation between high road density and landslide initiation (Pawłuszek et al. 2019).

I combined all seven raster layers described above in ArcGIS Pro using the Composite bands tool. The result was a multi-band raster image similar to those used in multispectral image analysis. Each raster input became a different band.

Supervised Classification

I decided to attempt a classification using only two classes, Landslide and Non-Landslide. I selected a random subset of 195 features (70%) from the slope movement polygons to serve as training samples for the Landslide class. For the Non-Landslide class, I collected 66 statistically uniform training samples of different sizes. I attempted to capture a variety of terrain types in these samples, including broad flat swaths of land modified for farm fields, riverine features that did not co-occur with landslides, steep slopes with a texture suggestive of exposed rock, and many more.

I chose to use the Support Vector Machine (SVM) classifier. SVM is a machine learning method used primarily for classification purposes. In a dataset of the pixel values from the raster composite image, this method finds and uses an optimal plane to separate pixel values into the two classes.

I made three attempts at classifying the study area. The first attempt was an exercise in understanding the mechanics of classification with elevation data. It included segmentation, a crucial step in OBIA. This first classification was only performed on the hill-shade DEM-derivative. The second classification was performed on the multi-raster composite map. It suffered an unknown issue that caused either splitting or duplication of training samples. Out of

caution, I performed a third supervised classification with slightly different training samples that represent a true 70% (by number of features) of the slope movement outlines. This final classification is the focus of the results.

Results and Error Assessment

This study does not follow the conventional calculations of accuracy and error often seen in imagery-based land cover classifications. The approach taken here assesses pixels in groups instead of at randomized points.

For the calculation of accuracy in the Landslide class, I focused on the landslide test polygons, which made up 30% of the original slope movement outline dataset. Within those polygons, I tabulated the total pixels, then calculated the percentage of those pixels that were correctly classified as Landslide, as well as the percentage incorrectly classified as Non-Landslide.

For the calculation of accuracy in the Non-Landslide class, I extracted all pixels in the classification that did not participate in any training sample polygons, and also were not part of the Landslide test dataset.

The river and road networks were examined in greater detail in the hopes of identifying patterns that would be helpful for the next classification. Since my interest was in the general relationship between roads and landslides in this area, I chose to analyze the road centerlines directly, rather than the road density map used in the classification, as they allowed for a simpler methodology.

For roads, I generated eleven 300 m wide bands, each representing progressively further ranges of straight-line distance away from the roads (the furthest band was stretched to 3337 m to include the maximum distance a landslide pixel could be from the road). I then converted these bands to multipart polygons (one polygon per distance range) for the purpose of overlay analyses. Within each band, I used the Tabulate Area tool to count the number of pixels by class, which was used to calculate the percentage of each polygon that was occupied by the Landslide class. For the purposes of comparison, I repeated the same steps using an idealized classification. This idealized classification (Figure 6.) is simply a rasterized version of all original slope movement outline polygons. The area contained within the polygons was classified as Landslide, while all other areas were classified as Non-Landslide. The idea was to find a relationship between the density of landslides and distance from roads in verifiable landslide data, and then compare that relationship to my classification. The methodology for examining the river-landslide relationship was very similar. The starting river layer was the raster network that I created. This analysis broke the distance into 13 bands, each 50 m in range.

Results

Within the test polygon subset, 71.9% of pixels were correctly classified. Non-Landslide pixels accounted for 28.1% of that subset; this percentage represents errors of omission from the Landslide class.

Within the test Non-Landslide area, 52.5% of pixels were correctly classified as Non-Landslide, while 47.5% were incorrectly classified as Landslide. The latter percentage represents errors of commission within the Landslide class.

Classification values were extracted for each process point. Out of the 3,351 process points, 3,066 (91%) were correctly classified as Landslide (Figure 5.).

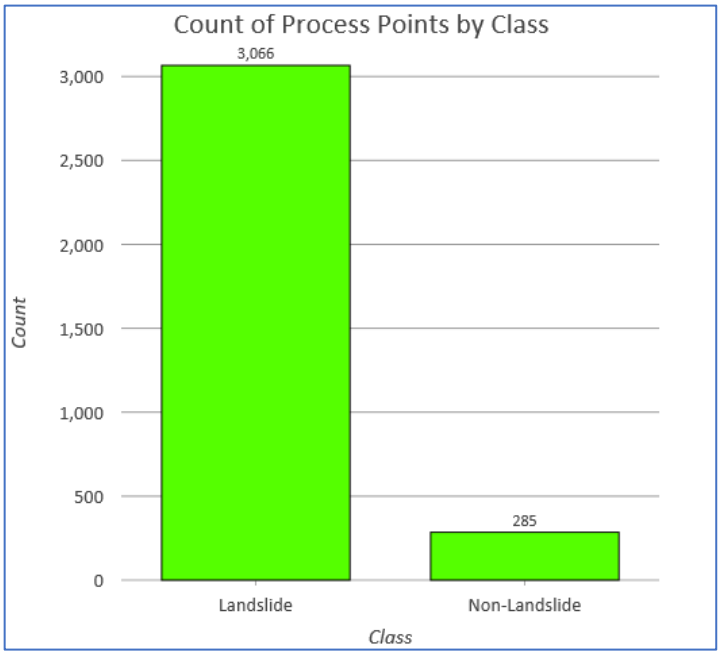

Figure 5. Process points counted by class.

In Figure 6., this classification is compared to an idealized classification. This latter classification uses pixels extracted from the original slope movement polygons to delineate the Landslide class. The remaining area has been reclassified into the Non-Landslide class.

In comparison to the idealized classification map, the classification map produced by this study shows a far greater Landslide class area (Figure 6.), which is consistent with the error statistics within the Non-Landslide test area of the map. While the Landslide class pixels are distributed throughout the full extent of the map, Sherando Quadrangle appears to contain a higher proportion of false positives than Horseshoe Mountain. This is a purely visual observation, as pixel totals have not been compared between the two quadrangles.

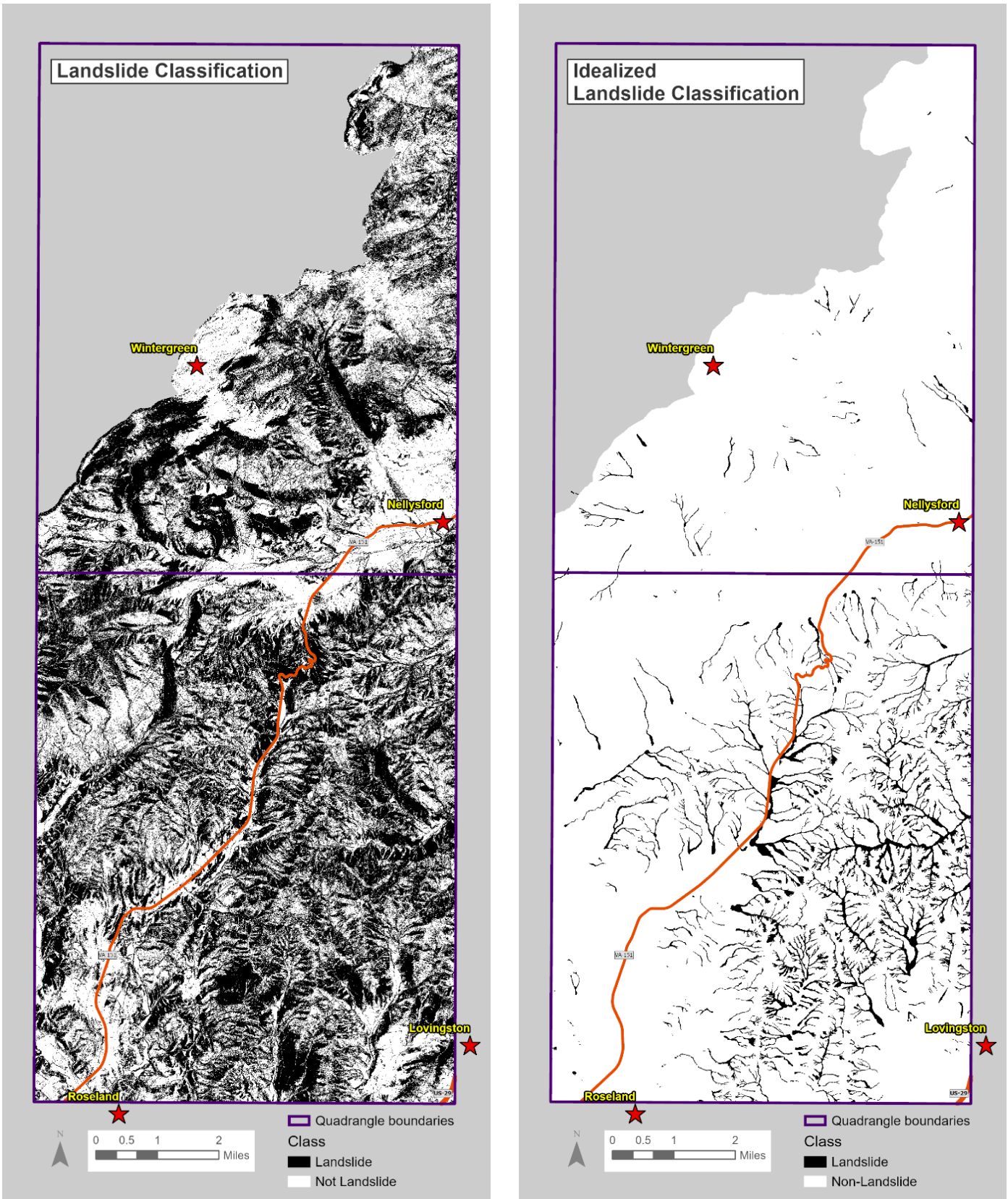

Figure 6. Left, the landslide classification map created by supervised classification. Right, an idealized classification created from slope movement outline polygons.

These falsely classified Landslide areas appear in Sherando as laterally continuous along hillslopes with few breaks in class. The Landslide pixels in an example from Sherando (Figure 7.) form a NE-SW trending wall. This pattern would be unusual for the debris flows in this area, which typically follow a far more dendritic pattern composed of individual chutes. Notice the same area viewed in a hill-shade map shows a pockmarked, craggy texture that also extends continuously along the hill slopes. The texture is potentially responsible for the entire slope being classified as Landslide.

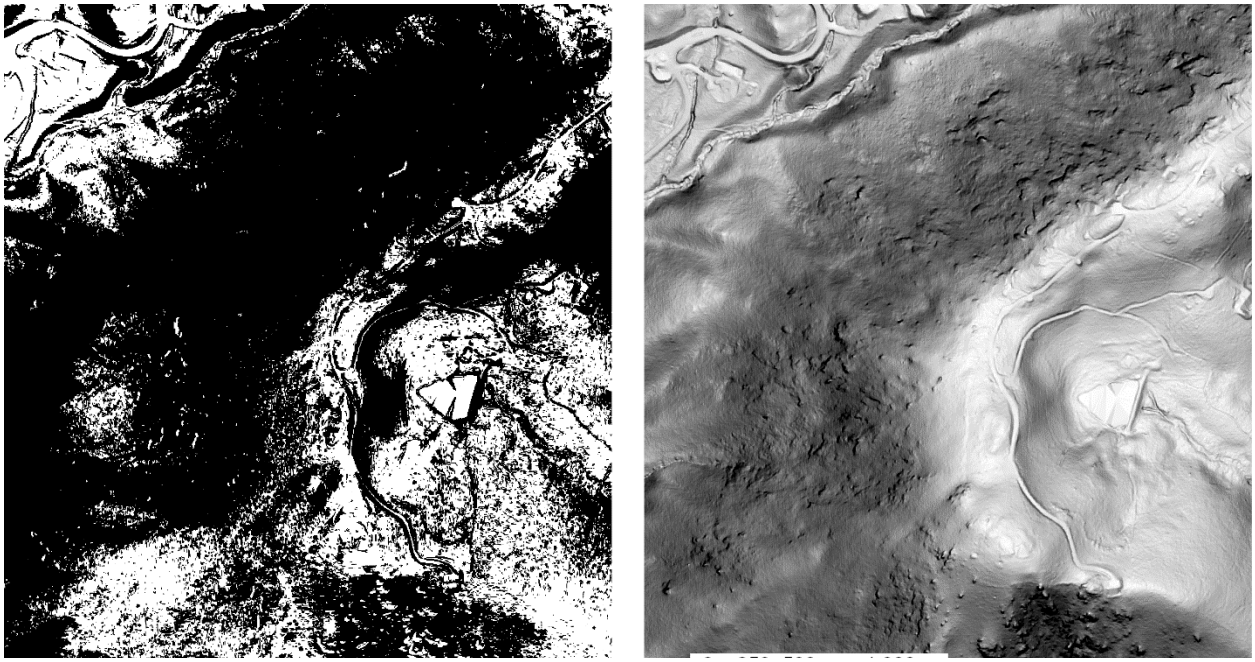

Figure 7. Left, a laterally continuous landslide deposit shown in classification. Left, the same area in a hill-shade map.

Some misclassified areas appear to be caused by specific, discrete features. In another part of Sherando, long, linear features classified as Landslide appear to follow the natural contours of the slope (Figure 8.). If these pixels were actual landslides, we would expect them to crosscut these natural contours as material flowed downslope. In the hill-shade map, the sharp edges of these features imply a human origin. These features may be old logging roads. The classifier has identified this pattern and placed it in the wrong category.

Other discrete misclassifications appear throughout the full extent of the map. Commonly identifiable misclassifications include, but are not limited to, ponds, breaks or fence lines between agricultural fields, highways, and local roads.

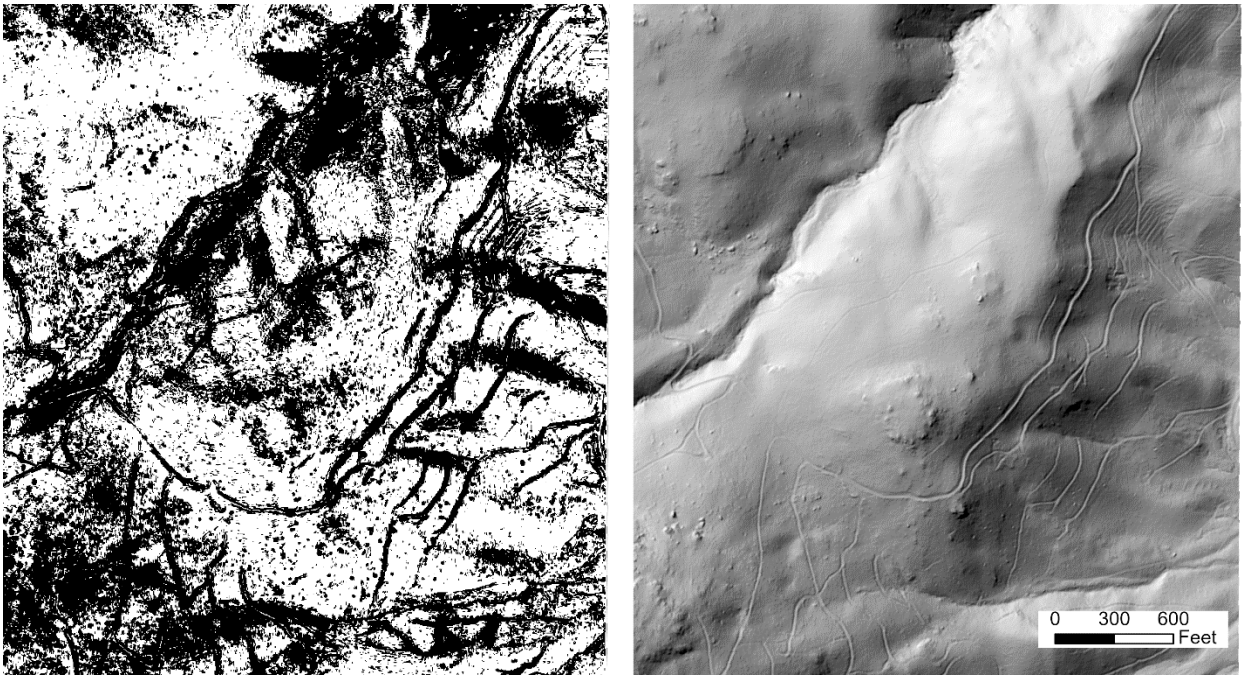

Figure 8. Left, Linear features that follow the path of hillslope contours. Right, the same linear features in hill-shade view.

Roads and Rivers

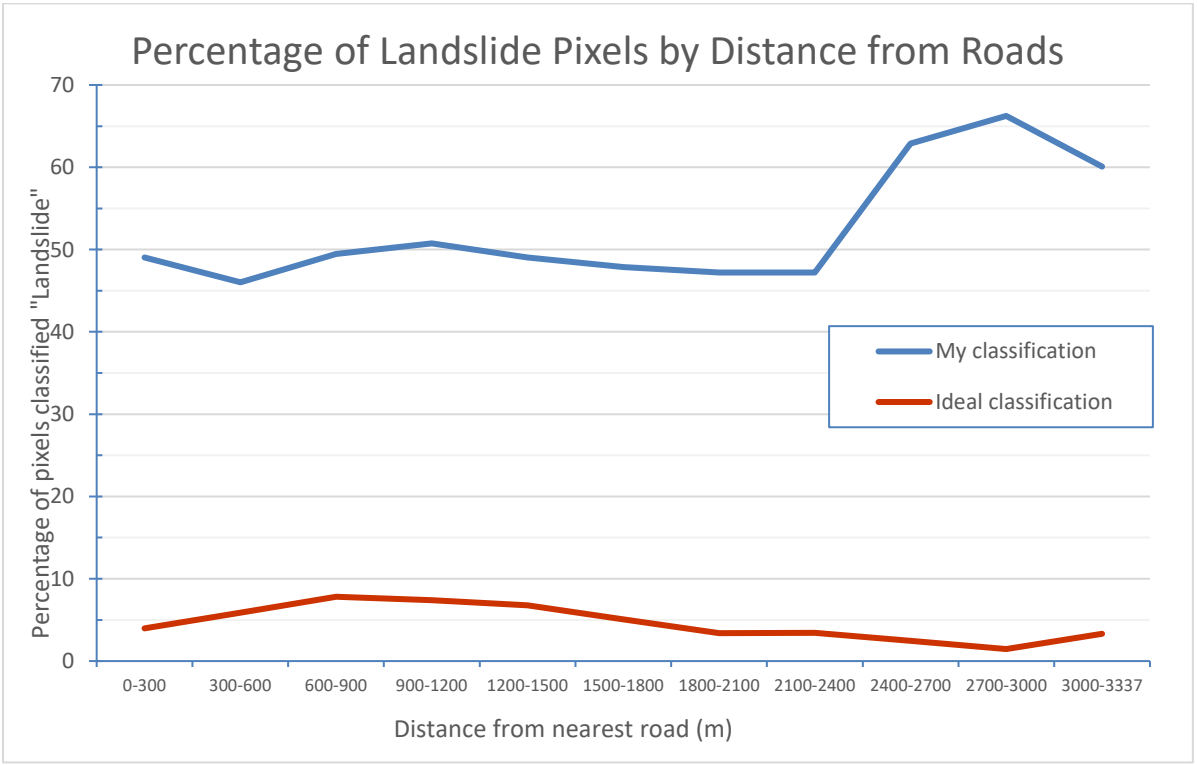

Figure 9. Pixel percentages at certain distances from the nearest road, compared by classification.

Figure 12. shows a visualization of the road distance bands described here. The following results relate to the chart in Figure 10. In the idealized classification, the peak percentage of landslide pixels occurs at 600-900 m from a road. The overall pattern is relatively flat, with a slight inverse relationship. In my classification, the value at each band is at least 40 percentage points higher than that of the idealized line. This is a result of the high number of misclassified Landslide pixels across the entire map. The pattern is similar in shape to an idealized classification, except for the slight peak in the 0-300 m band and the much more extreme rise and peak between 2100-2400 and 3000-3337 m band. If the trend had remained similar to the ideal classification, we would expect to see landslide percentages below 50%. Instead we see a high point at 66%. This could be partially explained by the smaller area of bands further away from roads. Because these bands have fewer pixels, it would take fewer poorly placed false positive landslide features to skew the percentage artificially high than in larger bands. Although percentages are inherently normalized, in this case for area, pixels in small bands carry more weight.

Pattern differences between my classification and the idealized classification in the first band suggest that the classifier is not finding the same relationship between landslides and roads as would be expected. This preliminary analysis of the idealized classification suggests that the correlation between landslides and distance from roads is weak in this study area.

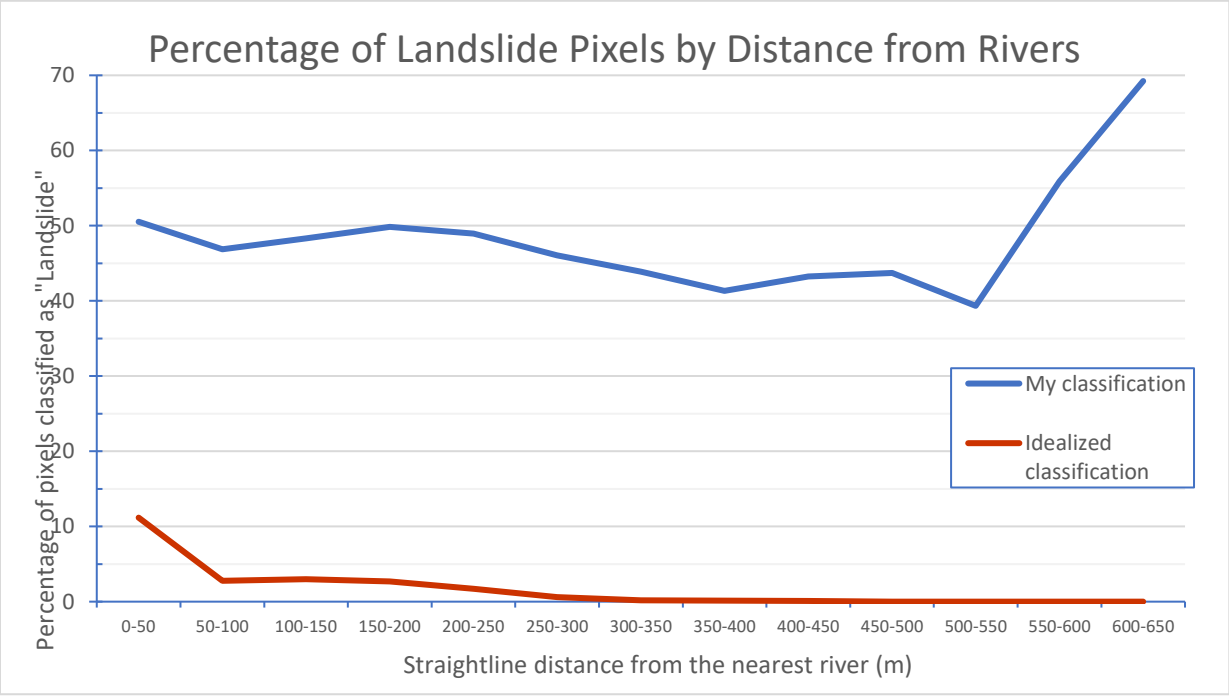

Figure 10. Pixel percentages at certain distances from the nearest river, compared by classification.

Figure 12. shows a visualization of the river distance bands described here. The following results relate to the chart in Figure 11. My classification again features much higher percentages, again

because of false positives. A similar rapid rise in percentage occurs beginning at 50-550 m from the nearest river. This rise may occur for the same reason seen in the roads analysis. The overall trend suggests an inverse relationship limited to the first 50 m away from a river, followed by a weaker inverse relationship that tapers off at 300-350 m. Beyond that band, the percentage of landslide pixels is close to 0. Excluding the peak beginning at 500-550m, my classification displays two peaks at 0-50 m and 150-200m. Again, the relationship between rivers and landslides is not the same in the two classifications. In both cases, it is possible that the classifier is finding a different relationship because it is finding stronger statistical relationships between landslide pixels and other factors, such as slope. Also, the training samples selected for this classification may have more heavily weighted factors like slope, while poorly representing road density and the presence or absence of rivers.

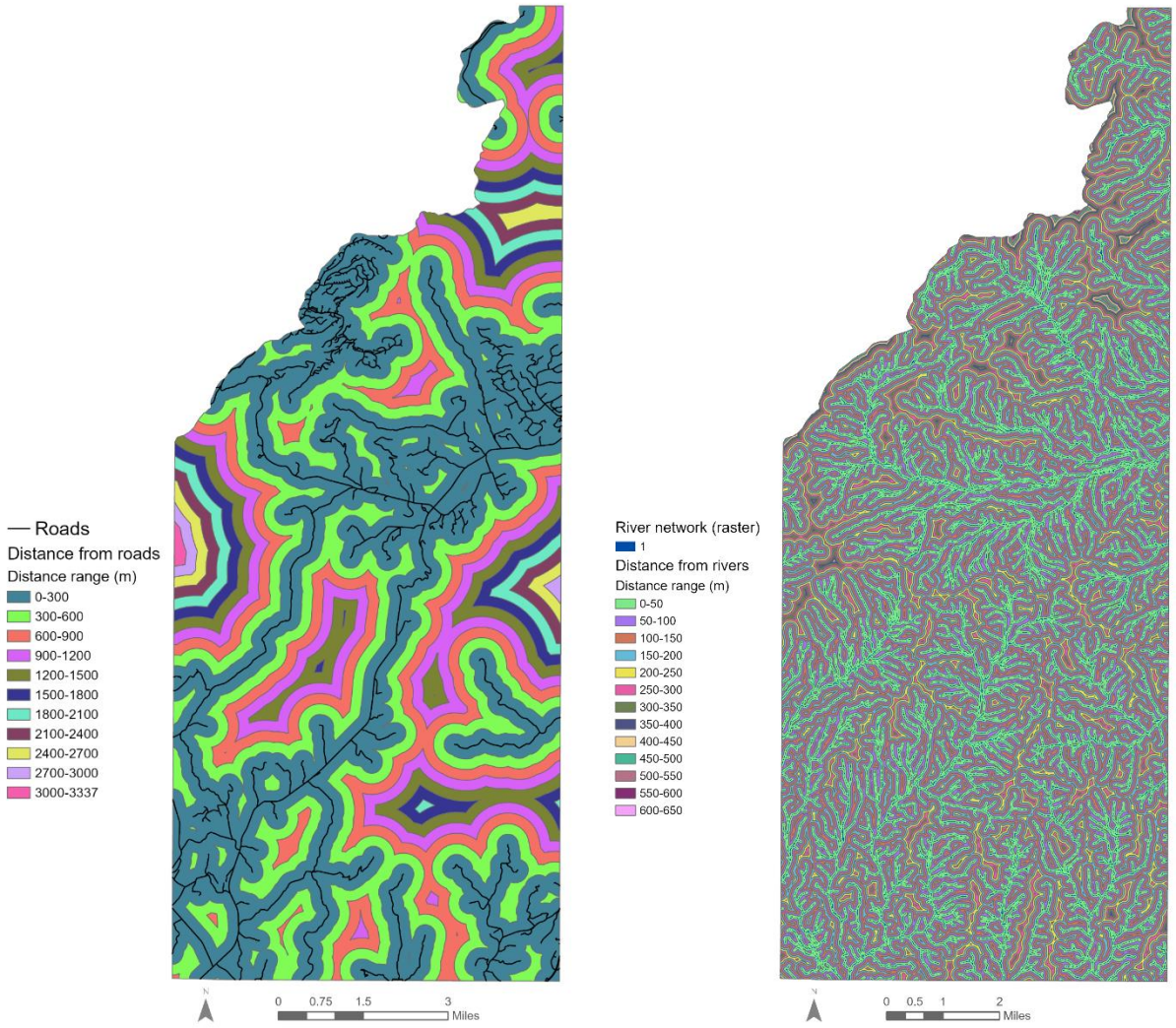

Figure 12. ***Left,*** **a map of the 300 m wide concentric bands originating at roads.** ***Right,*** **a map of concentric 50 m bands originating at rivers.**

Discussion

Although at face value an accuracy of 71.9% Landslide pixels correctly identified seems high, the usability of this map is lowered by the high number of falsely identified Landslide pixels. A preferable classification would strike a better balance between errors of commission and omission. An ideal classification would have lower values for both.

The appearance of a higher number of these false positives in the Sherando Quadrangle may be a result of imbalanced training sample collection. Horseshoe Mountain contains a higher density of landslides, and thus a higher proportion of Landslide training samples were collected from that quadrangle; the same quadrangle also contained the majority of Non-Landslide training samples. It is possible that the classifier was better able to distinguish between Landslide and Non-Landslide areas of Horseshoe Mountain because of this higher proportion of both types of samples. This is relevant because of the differences between the quadrangles. The classifier was better equipped to find differences in the steep slopes and rugged, rocky surfaces of Horseshoe Mountain over the comparatively flat, smooth, and more modified slopes of Sherando.

Across the entirety of the map, the classifier may have struggled to classify Non-Landslide pixels because of the large variety in landforms that compose this class. I captured a large variety of training samples, but the results were probably not representative of the full range of pixels encountered by the classifier. After all, in an idealized classification of this area, 94% of the map falls into the Non-Landslide class. There are a couple of solutions to correct this. One is to simply collect a wider variety of training samples. Another is to remove obvious Non-Landslide areas, such as ponds and farm fields from the map before classification begins. That way the classifier would start out with a narrower range of pixel values to classify.

Another major source of error in this study is the discrepancy between the Landslide training samples and the features visible on 2016 LiDAR-based DEMs. These slope movement outline polygons were drawn in part from historical aerial photography and orthophotography, as well as maps compiled from field-verified sources and DEMs of the past. These slope movement outlines in some cases represent the downslope extent of landslide feature deposits that were eroded or otherwise erased by 2016. However, the Landslide training samples were not refined or adjusted to reflect this difference. This introduced erroneous Landslide pixel values before classification, because the samples cover extraneous areas that no longer contain landslide deposits at all.

Certain changes could be made to strengthen, improve, or alter this study. One common method of landslide monitoring is change detection, in which precise changes of the landscape are quantified over time. Change detection in this area would likely rely on aerial imagery or even topographic maps. Although aerial photography of Nelson County from before 1969 likely

exists, the coarser scale and resolution would present difficulties in analysis. If change detection is not feasible, future workers may instead use aerial imagery to more closely mimic visual interpretation of landslide features. The benefits of automation may still be reaped if the imagery can be assimilated into the modeling process. Although capturing the original "footprint" of these deposits was not the focus of this study, a model that does attempt to capture them may be more useful for landslide susceptibility and inundation modeling down the road.

Apart from imagery, different DEM-derivatives and raster layers could easily be used with the methodology laid out in this study. The layers used here were chosen to fulfill the triple requirement of accessibility, time, and common use in previous studies. A couple of examples of DEM-derivatives that I wanted to include, but could not are "Openness": a measure of a given feature's enclosure or dominance compared to surrounding terrain (Yokoyama, Shirasawa and Pike 2002), as well as "Surface Relief Ratio": the difference between planimetric surface area and surface area that accounts for terrain (Jenness 2004). A significance assessment would better inform me as to which layers contributed the most to the classification.

In terms of Non-DEM-derivatives, the roads layer used in this study could be improved by the addition of informal roads, such as logging roads, in a largely rural area such as Nelson County. The supposed relationship between road density and landslide initiation becomes less relevant if the only roads considered are in areas unlikely to experience a landslide because of flat topography or extreme land modification and slope stabilization. Including a broader definition of roads might change the weak inverse relationship between distance from roads and landslides seen in the idealized classification.

After examining the relationship between rivers and landslides briefly in this study, I think the connection warrants further investigation, especially given the high density of streams over this study area. Streams will naturally exploit channels like the ones carved by landslides; many first and second order streams are visible in landslide features on a slope-shade map. Part of this study was looking at the likelihood of a landslide being near a river. The next step would be to examine the probability that a river is near a landslide.

Given the size and variability both within and between individual landslide features in this area, a pixel-based approach to classification may have not been an appropriate choice. The fine resolution of the LiDAR-based DEMs means that even small landslide features are larger than the pixel size. The strength of OBIA is its ability to group together pixels into cohesive "segments" before classification. Segments can be adjusted to represent real-world features; the segments preserve the relationship between pixels throughout the classification process. This is ideal for the multi-pixel sized landslides in this area.

A pixel-based approach, in contrast, means that instead of multi-pixel, real-world features being treated as individuals, pixels themselves are instead treated as individuals. Each pixel is not part

of a feature beyond the class that it is placed into during classification. This approach can work well for continuous swaths of discrete features, such as in the production of a land cover classification map. However, landslide features, even within just 1-2 types of landslides, exhibit variability in geometry and texture, both between separate features and within a singular feature. Factors such as slope and roughness may vary significantly within the extent of one debris flow. The shape and texture of landslides also change over time, as parts of the original deposits are eroded by recent streams or weathered by the regrowth of vegetation. A classification of these landslides would benefit from being able to treat groups of variable pixels as a whole feature. The OBIA method was effectively used in previous studies in other locations (Blaschke, Feizizadeh and Holbling 2014, Pawłuszek et al. 2019). OBIA is recommended for future researchers attempting to classify the full extent of landslide features in this area, from head scarp to downslope deposit.

If polygons are not a necessity of future classifications, the successful classification of process points suggests that focusing only on the initiation points of landslides may yield a more successful classification. Debris flow head scarps have a distinctive, steeply sloped, half-cone shape that is useful in the manual identification of landslide features in LiDAR-based slope-shade maps. This shape is consistent across features and would be easier to classify than extensive, variable landslide tracks and deposits. If the goal is finding a starting point for a landslide inventory, a more accurate classification of just initiation points is more trustworthy and useful than an inaccurate map of entire landslide features.

Conclusion

This landslide focused classification contains too many areas of falsely identified landslide pixels to be useful as the beginnings of a landslide inventory. Capturing more Non-Landslide training samples is one specific action that could lead to immediate improvement. Eliminating obvious Non-Landslide areas before classification would theoretically lead to more accurate results. Apart from Non-Landslide areas, Landslide training samples also require improvement. The main issue to address is the mismatch between the downslope extents of the slope movement outlines, and the current eroded extent of the same features visible in hill-shade maps. These polygons could be refined to exclude deposits that no longer exist.

The relationship between landslide features and rivers in this study area may yield insight that could be useful in future classifications if it is further explored. Based on the weak inverse relationship between distance from roads and landslide features in the idealized classification, roads may not have contributed meaningful data to this classification. A different relationship may exist between landslides and a measure of road density that includes abandoned and informal roads.

A more thorough examination of DEM-derivative values at all process points before classification may have helped to rule out or select the best set of derivatives. It is also recommended that future studies limit the scope to include only process point locations during the classification process instead of polygon features, at least during an initial classification. If landslide features must be captured in continuous areas, then I would recommend the implementation of OBIA over the pixel-based approach.

The highly variable nature of landslide features directly contributed to the low accuracy of this classification, but careful selection of raster layers, training samples, study area, and classification approach may lead to future successes given the same data.

References

Blaschke, T., B. Feizizadeh, and D. Holbling. 2014. Object-Based Image Analysis and Digital Terrain Analysis for Locating Landslides in the Urmia Lake Basin, Iran. IEEE Journal of Selected Topics in Applied Earth Observations and Remote Sensing 7 (12):4806-4817.

Grohmann, C., M. Smith, and C. Riccomini. 2011. Multiscale Analysis of Topographic Surface Roughness in the Midland Valley, Scotland. IEEE Transactions on Geoscience and Remote Sensing 49 (4):1200-1213.

Highland, L., and P. Bobrowsky. 2008. The landslide handbook. Reston, Va.: U.S. Geological Survey. 1-42.

Jenness, J. 2004. Calculating landscape surface area from digital elevation models. Wildlife Society Bulletin 32 (3):829-839.

Moosavi, V., A. Talebi, and B. Shirmohammadi. 2014. Producing a landslide inventory map using pixel-based and object-oriented approaches optimized by Taguchi method. Geomorphology 204:646-656.

Pawłuszek, K., S. Marczak, A. Borkowski, and P. Tarolli. 2019. Multi-Aspect Analysis of Object-Oriented Landslide Detection Based on an Extended Set of LiDAR-Derived Terrain Features. ISPRS International Journal of Geo-Information 8 (8):321.

Usgs.gov. n.d. Landslides 101. [online] Available at: <https://www.usgs.gov/natural-hazards/landslide-hazards/science/landslides-101?qt-science_center_objects=0#qt-science_center_objects> [Accessed 23 July 2020].

Virginia Department of Mines, Minerals, & Energy. Hurricane Camille 35-mm Slide Collection [Accessed May 2019]

West Virginia Statewide Hazard Assessment - Landslide Risk Assessment, presented 2019.

Yokoyama, R., M. Shirasawa, and R. Pike. 2002. Visualizing Topography by Openness: A New Application of Image Processing to Digital Elevation Models. PHOTOGRAMMETRIC ENGINEERING & REMOTE SENSING, 257-265.